Scanning tunneling microscopy and x-ray photoelectron diffraction investigation of C_{60} films on Cu(100)

M. Abel,[1] A. Dmitriev,[1] R. Fasel,[2] N. Lin,[1] J. V. Barth,[3] and K. Kern,[1,3]
[1]*Max-Planck-Institut für Festkörperforschung, Heisenbergstraße 1, D-70569 Stuttgart, Germany*
[2]*Swiss Federal Laboratories for Materials Testing and Research (EMPA), CH-8600 Dübendorf, Switzerland*
[3]*Institut de Physique des Nanostructures, Ecole Polytechnique Fédérale de Lausanne, PHB-Ecublens, CH-1015 Lausanne, Switzerland*
(Received 28 October 2002; published 9 June 2003)

Ultrathin C_{60} films grown on a Cu(100) surface in ultrahigh vacuum have been investigated by scanning tunneling microscopy (STM) and x-ray photoelectron diffraction (XPD). STM observations show that following deposition at room temperature C_{60} molecules decorate substrate steps and order in densely packed extended islands and layers. Two kinds of contrast, i.e., different apparent heights, are encountered in the film evolution, which are associated with substrate reconstruction and inequivalent C_{60} bonding. At elevated temperatures (500–600 K) a striped regular $\binom{10\ 6}{0\ 4}$ superstructure is obtained comprising two distinct C_{60} species. From an XPD analysis of this phase the corresponding possible C_{60} bonding configurations could be determined.

DOI: 10.1103/PhysRevB.67.245407 PACS number(s): 68.65.−k, 68.43.Fg, 68.43.Hn

I. INTRODUCTION

Since the discovery of C_{60}, many studies have been performed in order to understand the basic properties of this complex molecule and develop possible applications. An important issue concerns the fabrication of low-dimensional systems incorporating C_{60}, where intriguing phenomena have been observed, such as Fermi gap opening in the C_{60} monolayer on Ag(100) (Ref. 1) or superconductivity at alkali metal doped C_{60} surfaces[2] at low temperatures. Consequently fullerene-surface interactions have attracted much interest.[3–5] On metal surfaces, C_{60} molecules in general have the propensity to accept electrons from the substrate, and this charge transfer is in part responsible for the structural and electronic properties of the overlayers. Furthermore, the bonding geometry, the detailed arrangement of the C_{60} molecules within the films and their intermolecular distances play a decisive role.

Due to its extremely high spatial resolution, scanning tunneling microscopy (STM) has been widely used to investigate the molecular bonding, nucleation and growth processes and film morphologies of C_{60} deposited on metal[6–20] or semiconductor surfaces.[21–25] Quite frequently in the STM studies distinct C_{60} species were discerned, i.e., molecules appearing with different imaging heights or intramolecular features. Since STM images a convolution of the surface electronic and geometric structure, it is often controversial as to whether the contrast is related simply to a difference in geometrical height (e.g., due to surface reconstruction) or to electronic effects (e.g., a spatially non-homogeneous density of states due to different adsorption sites or cage orientations). On the other hand, x-ray photoelectron diffraction (XPD) has proven to be a powerful means to determine the orientation of the C_{60} cage at surfaces.[7,10,16,26] An XPD analysis of C_{60} films is thus an important part to develop a detailed understanding of their electronic or vibrational properties obtained by other methods.

Here we report a combined STM and XPD investigation on C_{60} films grown at room temperature on a Cu(100) surface under ultra-high vacuum conditions. The coverage range 0.15–1.5 ML was investigated by STM (a ML is defined as 1.15 C_{60} molecules per nm^2, corresponding to a close-packed saturated molecular layer). The evolution of the films was followed in detail and there is evidence for inequivalent molecular bonding and thermally activated substrate restructuring. At elevated temperatures a highly regular striped superstructure was obtained. Its unit cell was determined to $\binom{10\ 6}{0\ 4}$ both by STM and low-electron energy diffraction (LEED) observations. An XPD analysis of this superstructure was performed to determine the possible C_{60} bonding configurations. From the combined analysis it is suggested that two distinct C_{60} species are involved.

II. EXPERIMENT

The experiments were performed in two different ultrahigh vacuum chambers. The Cu(100) surface was cleaned by repeated cycles of Ar^+ sputtering and annealing (800 K), allowing one to obtain atomically flat terraces of up to 100-nm width separated by monoatomic steps. Commercially available C_{60} in powder form (purity: 99.99%) was deposited from a Knudsen-cell type evaporator. For the STM experiments the temperature of the cell was maintained at 670 K during the evaporation (corresponding evaporation rate: 0.03 ML/min) whereas the substrate was held at 300 K. A home-built variable temperature beetle-type STM operational in the temperature range 40–800 K was employed (system base pressure $\sim 3\times10^{-10}$ mbar). The STM data were obtained in the constant current mode, with maximum bias voltages up to 3 V. The XPD and LEED experiments were performed at the University of Fribourg's VG ESCALAB Mark II spectrometer equipped for motorized sequential angle-scanned data acquisition.[27] Mg $K\ \alpha$-excited photoelectrons were analyzed with a 150-mm-radius hemispherical analyzer. Highly ordered C_{60} monolayers were obtained by depositing two or more monolayers onto the sur-

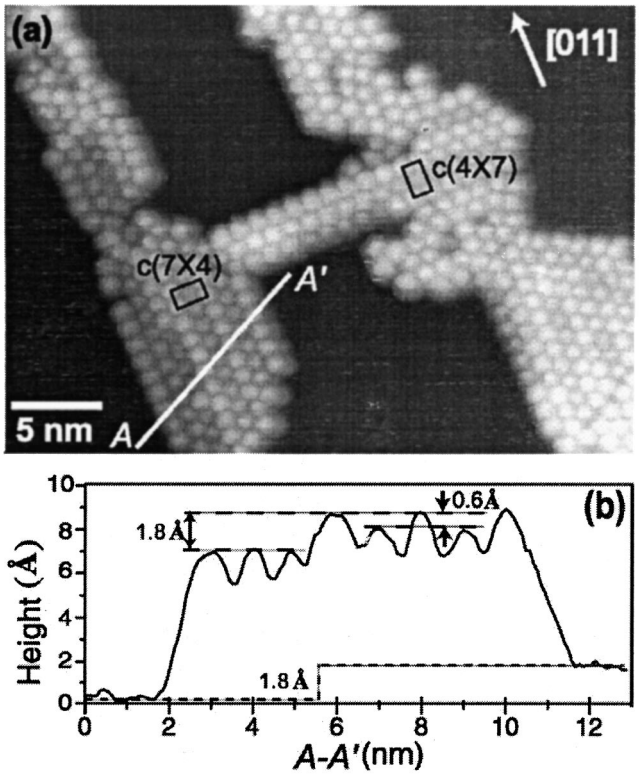

FIG. 1. (a) STM image of Cu(100) following deposition of 0.15 ML C_{60} at room temperature ($U=0.5$ V, $I=0.2$ nA). The molecules decorate both upper level and lower level step edges. Striped arrangements are formed which can be described by a local $c(4\times7)$ unit cell (respectively $c(7\times4)$ for the 90° rotational counterpart). (b) STM contour plot along the points A and A' indicated in (a). The 1.8-Å Cu(100) step height is encountered across the C_{60} islands. The underneath Cu(100) monoatomic step is depicted by a dotted line and the 0.6-Å height difference of the two C_{60} species is marked.

face held at room temperature and subsequent annealing above the C_{60} sublimation temperature of 575 K for a few minutes.

III. RESULTS AND DISCUSSION

A. STM observations on the evolution of C_{60} films

The STM image reproduced in Fig. 1 reveals that upon deposition of small C_{60} doses at room temperature, the molecules diffuse to the steps, where they nucleate at both upper and lower step edges and form islands. Preferential nucleation at step edges for C_{60} films at 300 K has been similarly reported for other noble metal substrates such as Ag(111),[28] Ag(100),[29] Au(111),[30] and Cu(111).[21] In contrast, for the case of Ag(110),[31] Cu(110),[8] and Pd(110),[15] homogeneous nucleation on the surface occurs, which is associated with stronger molecule-substrate interactions at these more open and highly corrugated surfaces.

Upon comparing the Cu(100) atomic structure with the C_{60} arrangement, we found that the close-packed fullerene molecules are organized in a faulted commensurable quasihexagonal manner [cf. Fig. 1(a)]. Bright and dim molecules

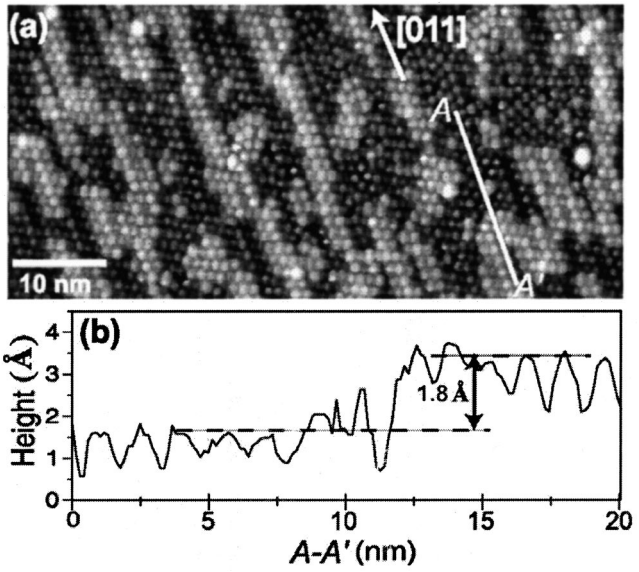

FIG. 2. (a) Nearly saturated C_{60} layer grown at room temperature with poor quasihexagonal ordering in anisotropic elongated domains in a two-level morphology. (b) The height difference between the domains in the C_{60} monolayer is 1.8 Å, which indicates limited substrate mass transport in the film evolution.

with a height difference of 0.6 Å are distinguished [see the STM contour line in Fig. 1(b)]. The imaging height of the bright (dim) species corresponds to 7.2 ± 0.3 (6.6 ± 0.3) Å, and thus is comparable to the hard sphere diameter (7.1 Å). Note that imaging heights of adsorbed C_{60} falling significantly below the diameter of the carbon atom cage are a typical finding, and values in the range 2–6 Å have been reported for various systems.[6–18] The molecules tend to form alternating bright/dim strings oriented along high-symmetry [011] or $[0\bar{1}1]$ crystallographic directions. The nearest neighbor (nn) lateral distances in the islands are in the range 9.8–10.3 Å, which comes close to the intermolecular distance of 10.02 Å in the close-packed plane of a C_{60} fcc crystal. This is a typical result for adsorbed C_{60} layers at metal surfaces.

The square symmetry of the copper substrate accounts for two equivalent domains with C_{60} strings mutually rotated by 90°. The ordering of the molecules in the bright/dim sequence can be described by a $c(4\times7)$ unit cell, as marked in Fig. 1(a). The strings usually comprise a maximum of ten molecules. The absence of long-range order is ascribed to kinetic limitations and the observed metastable situation is understood as a result from the subtle balance between lateral C_{60} intermolecular interactions and molecule-substrate interactions, with the first favoring close packing and the latter square symmetric arrangements.

With increasing coverage the C_{60} growth proceeds outwards from the saturated steps and large islands gradually extend over the terraces until the first molecular layer is completed upon island coalescence. The first layer as formed at a single Cu terrace at room temperature is shown in Fig. 2(a). It is a two-level system comprising upper- and lower-level domains with the poorly ordered striped phase, i.e., the 0.6 Å corrugated bright/dim row sequences introduced above. The STM contour line depicted in Fig. 2(b) shows that the height

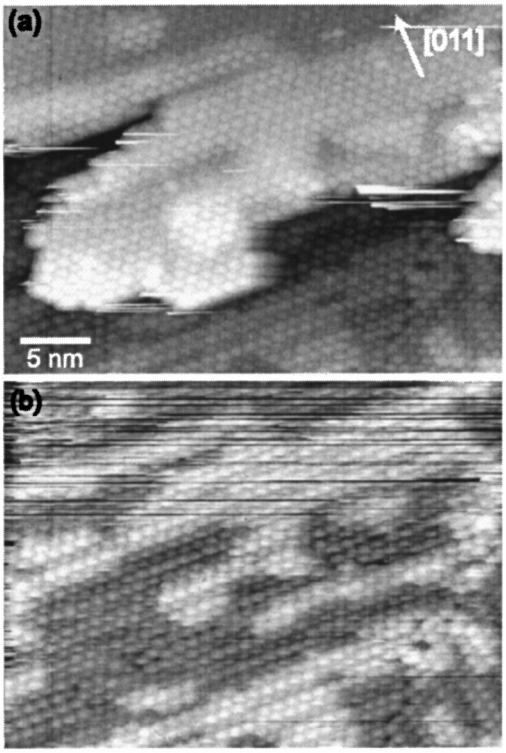

FIG. 3. (a) C_{60} film morphology following deposition of ~1.5 C_{60} ML at room temperature. Irregular second layer islands have formed, where quasihexagoal ordering persists. (b) STM image of the same area as (a) after the second C_{60} layer islands have been removed by scanning at a reduced tunneling resistance ($U = 0.1$ V, $I = 0.2$ nA). The morphology of the second layer is directly correlated with that of the first one.

difference between the domains is 1.8 Å corresponding to the substrate step. Roughly a third of the domains is at the upper terrace level. Since the domains do not reflect the morphology of the pristine substrate, this height difference is indicative of appreciable short-range substrate mass transport.

A further increase in the coverage gives rise to second layer formation. Upon room temperature deposition irregular islands form on the first layer which can be readily resolved by STM. It turned out that it is even possible to remove locally the second layer with the STM tip by scanning a small area at a low voltage. This is demonstrated by the data shown in Fig. 3. The images moreover reveal that the shape of the second layer anisotropic islands is encountered again in the first monolayer upon their removal. This indicates that the domain structure in the first layer geometrically induces that in the second layer.

Reasonably ordered coexisting first and second layer structures could be obtained upon deposition of 1.5 ML at room temperature and subsequent annealing at 500 K. The STM image shown in Fig. 4 reveals that compact islands are formed. In both layers a two-level morphology prevails, i.e., similar to the first layer structure, the second layer contains anisotropic domains with a 1.8-Å height difference (cf. the cross section $b\,b'$ and $c\,c'$ in Fig. 4; note that this feature is harder to discern in Fig. 3(a) where the gray scale range for image representation has been used for all terraces present in

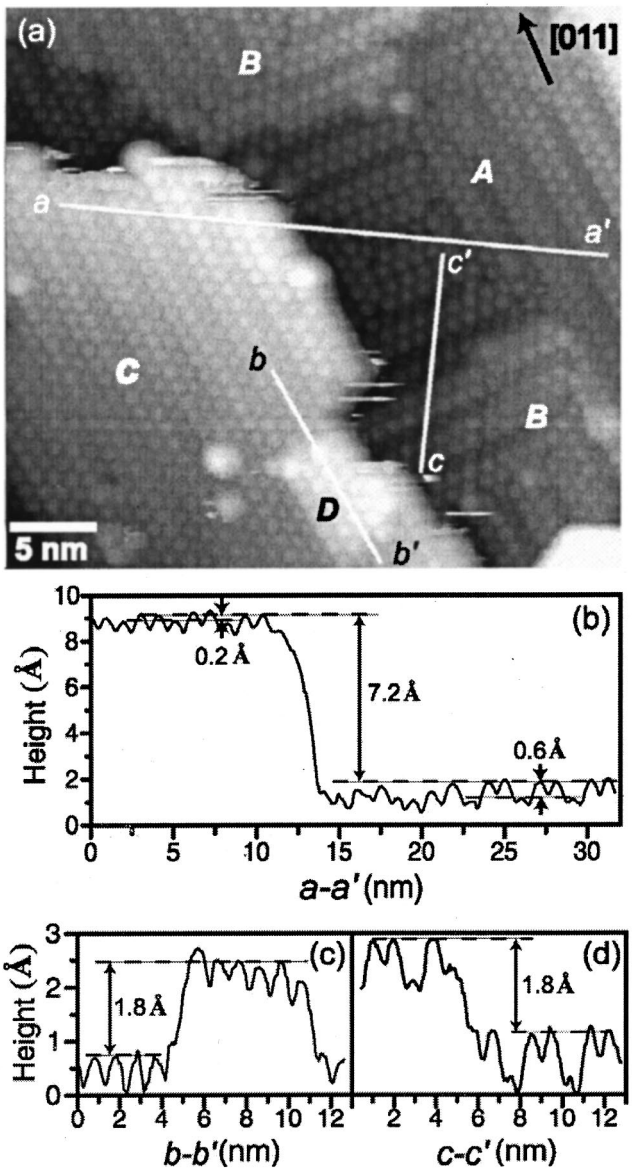

FIG. 4. (a) Compact second layer islands can be identified following deposition of 1.5 C_{60} ML at room temperature and annealing at 500 K. The upper-level domains (1.8 Å above the nominal layer planes) coalesce in islands for both the first (label *B*) and second C_{60} layer (label *D*). Striped arrangements prevail at the entire surface. (b)–(d) STM contour lines as indicated in image. Corrugation amplitudes amount to 0.6 Å for the first C_{60} layer (label *A*) and 0.2 Å for the second layer (label *C*), respectively.

the observed region). From the corresponding contour lines the mean height of the lower level in the second layer with respect to the nominal plane (corresponding to its lower level) of the first layer is determined to 7.2 Å (cf. the cross section $a\,a'$ in Fig. 4). This is defined as the nominal second layer plane. The second layer imaging height thus falls slightly below the interlayer distance of close-packed planes in the molecular C_{60} crystal, which amounts to 8.2 Å.

The data in Fig. 4 reveal, moreover, that a similar quasihexagonal molecular ordering prevails within all domains, i.e., the alternating rows form preferentially a superstructure

consisting of a sequence of two bright and one dim string. The superstructure exists in two 90° rotational domains. It can be found in both levels of the first molecular layer with 0.6-Å corrugation (labels *A* and *B* in Fig. 4) and in the second C_{60} monolayer (labels *C* and *D* in Fig. 4) with 0.2-Å corrugation (cf. cross sections *a a′* and *b b′* in Fig. 4). The large isotropic domains are attributed to the coalescence of the small anisotropic domains observed before annealing.

In the evolution of C_{60} films on Cu(100) thus distinct differences in the molecular imaging can be distinguished. On the one hand side there is a two-level morphology in both the first and the second C_{60} layer where islands protruding 1.8 Å (cf. Figs. 2 and 4) with respect to the nominal planes exist. On the other hand there is the 0.6 Å (0.2 Å) corrugation of bright/dim rows in the first (second) C_{60} layer. From the STM results it is not possible to directly distinguish whether or not differences in height in molecular imaging is due to the surface geometry or due to an electronic effect (increase of the local density of states). Nevertheless, the variation of the corrugation height of the first and the second C_{60} layer allows us to draw conclusions for the two kinds of contrast in the present system. Rowe *et al.*[32] showed by x-ray absorption spectroscopy and x-ray photoemission spectroscopy measurements that the electronic transfer from the copper substrate is more important for the first C_{60} layer than for the second. This may be used to discriminate between electronic and geometric contribution, because the substrate induced charge transfer effect should be smaller in the second C_{60} layer whereas the geometrical contribution is not expected to change. The 1.8-Å elevated domains are too low to represent a true C_{60} layer (C_{60} cage diameter is 7.1 Å). Considering that their height matches that of a Cu(100) monoatomic step, it can be safely concluded that the 1.8-Å raised domains are essentially due to a geometric effect, i.e., a rearrangement of substrate atoms. The 1.8-Å raised domains in the C_{60} layers are thus rationalized as containing an additional Cu layer underneath the C_{60} films, consisting of Cu atoms released in the formation of a substrate reconstruction at the C_{60} stripe arrangements. This is in accordance with the general tendency of C_{60} molecules to replace substrate atoms in order to form local reconstructions allowing for an increased adsorbate-substrate coordination.[9,14–16,33,34] That is, in Ag(100),[18,29] Pd(110),[15,16] and Ni(110) (Ref. 8) films C_{60} arrangements with 2-, 1.5-, and 1.3-Å height differences were encountered, respectively, which values correspond in all cases to the step height of the metal substrate. This interpretation is supported by the fact that (i) the domains coalesce upon annealing, which is associated with the coalescence of the underneath Cu islands and (ii) the domains on the first layer and on the second layer show the same 1.8-Å elevation.

The physical reasons underlying the smaller height differences of the bright/dim rows (cf. Figs. 4) must be of different origin since the corrugation is 0.6 Å at the first C_{60} monolayer and 0.2 Å at the second one. However, the 2:1 ratio for the number bright and dim rows in the superstructure unit cell indicates together with the observation that a similar domain height ratio was encountered under condition of limited surface mass transport in the monolayer formation (cf. Fig. 2) that only a fractional substrate layer has been displaced underneath the adsorbed C_{60} species in the first molecular layer. It is hence suggested that the bright and dim rows experience a different local substrate environment and may have distinct orientational and electronic configurations. The reduced 0.2-Å corrugation of the second layer C_{60} is understood as a result of the smaller charge transfer effect for the second layer molecules possibly along with relaxations in the C_{60} packing.[32]

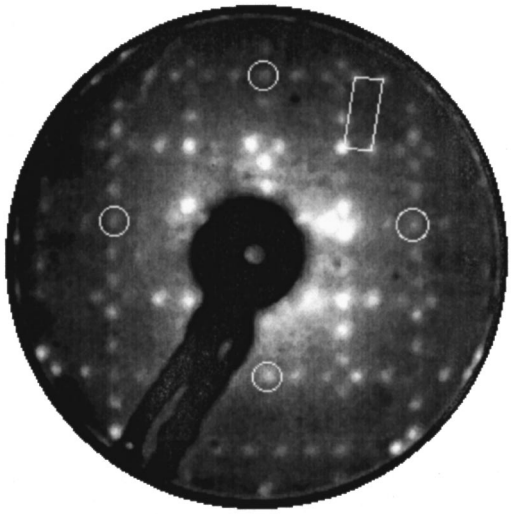

FIG. 5. LEED pattern ($E=30$ eV) of the regular C_{60} monolayer superstructure obtained upon tempering at 575 K. It results from the superposition of two possible rotational domains reflecting the square substrate symmetry: $\left(\begin{smallmatrix}10 & 6\\ 0 & 4\end{smallmatrix}\right)$ and $\left(\begin{smallmatrix}-4 & 0\\ -6 & 10\end{smallmatrix}\right)$. Half-order reflections and unit cell of one of the domains are indicated.

B. Combined LEED, STM, and XPD analysis of the monolayer superstructure

LEED observations of the tempered C_{60} monolayer reveal distinct reflections on a low background indicative of a well-ordered surface. A representative diffraction pattern obtained at 30-eV electron energy is reproduced in Fig. 5. It results from the superposition of the two rotational domains of the striped phase, which can be described by $\left(\begin{smallmatrix}10 & 6\\ 0 & 4\end{smallmatrix}\right)$ and $\left(\begin{smallmatrix}-4 & 10\\ -6 & 10\end{smallmatrix}\right)$ matrix notations, respectively.

STM data of this phase are in agreement with the LEED structure. In the STM image reproduced in Fig. 6(a), the corresponding real-space unit cell of the molecular film is indicated. The observed stripe arrangement consists again of one dim and two bright row sequences with a quasihexagonal molecular packing. The high-resolution data reproduced in Fig. 6(b) reveal, moreover, that intramolecular resolution can be obtained for the dim C_{60} rows, when small tunneling resistances are employed. For small positive tip bias voltages a three-lobe inner structure of the dim C_{60} appears whereas it is impossible to resolve any inner structure of the bright species [Fig. 6(b)]. Intramolecular C_{60} resolution with threefold symmetry have been observed similarly with C_{60} adsorbed on other substrates.[21,23] In particular, theoretical and experimental study of C_{60}/Cu(111) indicates that the density

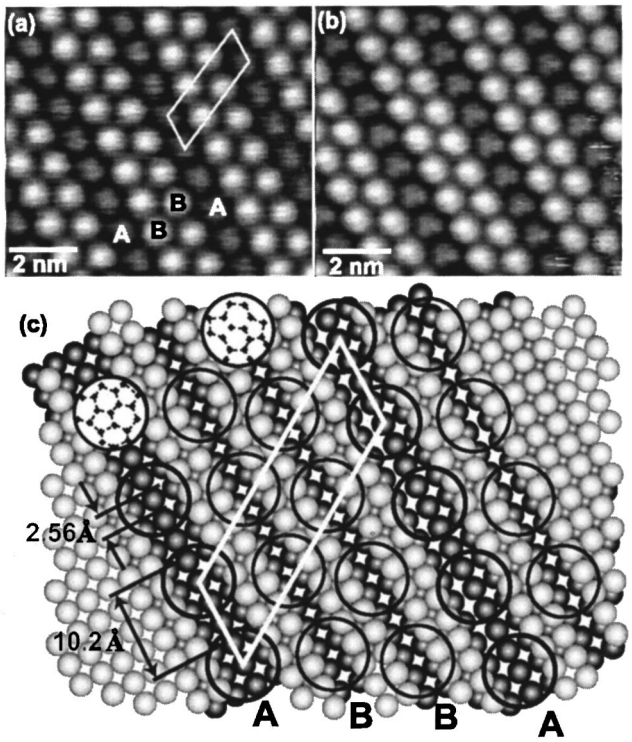

FIG. 6. High-resolution STM images of the striped C_{60} monolayer structure obtained after annealing a monolayer film at 500 K. (a) The $\binom{10\ 6}{0\ 4}$ unit cell in accordance with LEED is marked ($U=1.5$ V, $I=0.2$ nA). (b) At low tunneling resistances an internal molecular structure is resolved in the dim rows ($U=0.02$ V; $I=0.2$ nA). (c) Tentative real-space model for the corrugation of the striped phase and the inequivalent positioning of C_{60} molecules, assuming simple missing-row substrate reconstructions where minority (dim, labeled **A**) and majority (bright, labeled **B**) species reside at troughs with one and two substrate atomic rows removed, respectively.

of states are of doughnut shape for the highest-occupied molecular orbital and of threefold symmetry for the lowest unoccupied molecular orbital.[21] With the present system the intramolecular features signal that the electronic configurations and C_{60} cage orientations of the bright and the dim molecules are different and possibly the electron transfer is not the same for those two cases. This interpretation is in line with observations of C_{60} on Au(111), where spatially resolved scanning tunneling spectroscopy indicate subtle variations of the molecules' electronic properties depending on their bonding site at the substrate.[17]

A schematic model of the molecular layer is depicted in Fig. 6(c). It includes a tentative modeling of the suggested substrate reconstruction in its simplest imaginable form with the molecules placed in the troughs of two different missing-row structures, where for each bright (dim) molecular rows one (two) substrate rows are removed. This implies both a geometric difference in height and an inequivalent bonding to the substrate (note, however, that more intricate arrangements are feasible, similar to those described in Refs. 14 and 16). The intermolecular distance along the rows amounts to $4a=10.2$ Å (a is the Cu substrate atom nn distance) and the C_{60}-C_{60} distance for neighboring molecules of adjacent rows projected to the substrate plane is 10.3 Å. These values are typical for dense C_{60} layers at metal surfaces. Moreover it is apparent that the C_{60} positioning and size of the unit cell implies different adsorption sites for the bright (majority) and dim (minority) C_{60} molecules (note that this also holds in the case of additional substrate reconstruction). That is, assuming that the dim C_{60} molecules sit in fourfold hollow sites (label *A*), the two bright rows (label *B*) reside at nearby bridge sites. In a simple hard sphere model the corresponding geometrical height modulation between bright and dim rows would be 0.12 Å, significantly smaller than the 0.6-Å corrugation observed. Consequently, the observed contrast and difference in intramolecular resolution is associated with additional electronic effects and substrate reconstruction. Charge transfer between C_{60} and Cu surface was already recognized by photoemission experiments,[32] and here it may be nonequivalent for molecules of bright and dim rows, similar to findings with C_{60}/Au(111).[17] The detailed nature of the suggested substrate reconstruction cannot be conclusively addressed with the data at hand. However, since it is frequently encountered in C_{60} adsorption at metals and substrate mass transport occurred upon room-temperature deposition with the present system, it is likely that the substrate atoms rearrange in the formation of the regular striped phase in order to provide an optimized bonding geometry for the molecules. A similar behavior was recently deduced for the related C_{60}/Ag(100) system on the basis of STM observation.[18,19]

The experimental C 1*s* XPD pattern from a well-ordered monolayer of C_{60} on Cu(001) is depicted in Fig. 7(a). The C 1*s* intensity has been transformed into a linear gray scale with white corresponding to maximum intensity, while angles are projected stereographically: the center of the plot represents normal emission, and the outer circle corresponds to grazing emission along the surface plane. The mostly instrumental polar dependence of intensities has been removed by normalizing each azimuthal circle by its average intensity value. The marked diffraction features indicate that the molecules are not orientationally disordered but take distinct molecular orientations. Furthermore, the fourfold rotational symmetry of the XPD pattern excludes molecular orientations other than those exhibiting a onefold or twofold symmetry axis along the surface normal. C_{60} adsorption on five-membered rings (five-ring) or six-membered rings (six-ring) can, therefore, be excluded for this system.

In order to determine the C_{60} molecular orientation(s) giving rise to the XPD pattern an extensive *R*-factor analysis comparing the experimental pattern to single-scattering cluster (SSC) calculations has been performed. Details of the C_{60} SSC calculations and the *R*-factor analysis can be found in Ref. 26. In short, the orientation of a C_{60} molecule is varied on a dense grid of Eulerian angles (ϕ,θ,Ψ). For each orientation (ϕ,θ,Ψ) a SSC calculation is performed and compared to the experimental XPD pattern. The agreement is quantified by means of the *R*-factor RMP (where multipole coefficients of experimental and calculated diffraction patterns are compared),[35] and visualized in a stereographic *R*-factor plot.[26] In a first series of calculations, all molecules were

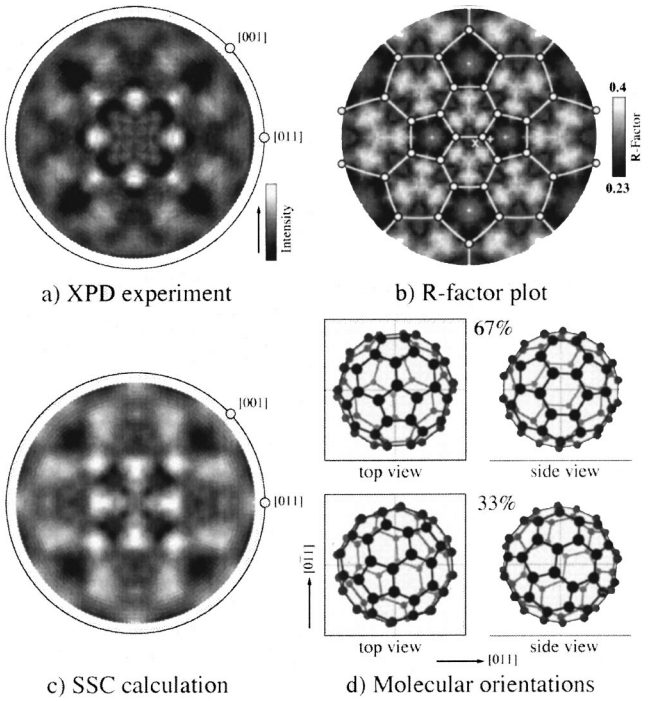

FIG. 7. (a) Experimental C 1*s* XPD pattern ($E_{\mathrm{kin}}=970$ eV) from the striped C_{60} monolayer structure. (b) Stereographic representation of the *R* factor obtained by systematically varying the orientation of the C_{60} molecular axis as well as the C_{60} azimuthal orientation in the SSC calculations (see the text for details). (c) Best-fit SSC calculation for 67% and 33% of the molecules in the orientations indicated in (b) by "+" (majority) and "×" (minority), respectively. (d) Illustration of the majority (top) and minority (bottom) molecular orientations.

assumed to be identically oriented apart from the four symmetry-equivalent azimuthal orientations due to the fourfold symmetric substrate surface. In other words, all C_{60} molecules were considered to be oriented with the same molecular axis perpendicular to the Cu(001) substrate surface. A stereographic grayscale representation of the resulting *R* factors is shown in Fig. 7(b). Each point of the plot gives the value of the *R*-factor when that particular molecular axis (ϕ,θ) of the C_{60} molecule is oriented perpendicular to the surface. The *R*-factor minimum (RMP is 0.23) is indicated by a "+" sign, and it can be seen that it is located close to an edge atom belonging to two 6 rings and a 5 ring. The best agreement with experiment is thus obtained for a C_{60} molecule with its onefold axis oriented almost along the surface normal, slightly tilted towards the bottommost 5 ring.

Motivated by the observation of bright and dim molecular species in the STM images of the close-packed monolayer structure, we included the possibility of two coexisting inequivalent molecular orientations in a second series of calculations. Indeed, the consideration of a possible second molecular orientation considerably improves the agreement with experiment, as indicated by a lowering of the *R* factor from 0.23 to 0.18. Interestingly, the best agreement is obtained with 67% of the molecules in the orientation discussed above and 33% in a slightly different orientation, indicated by an "×" in the *R*-factor plot [cf. Fig. 7(b)]. The two inequivalent molecular orientations are depicted in Fig. 7(d). The minority species also has its onefold axis oriented roughly along the surface normal, but in contrast to the majority species it is slightly tilted towards its bottommost 6 ring. More significantly, its azimuthal orientation differs from the one of the majority species by a rotation of 56° around the surface normal. The best-fit SSC calculation for 67% and 33% of the molecules in the respective orientations [Fig. 7(d)] is given in Fig. 7(c). It can be seen that it reproduces the experimental XPD pattern [Fig. 7(a)] rather well. The observation of two inequivalent molecular orientations with the same 2:1 relative weight as the bright and dim molecules in the STM images (Fig. 6) gives strong support for associating the bright (dim) molecular species with the majority (minority) molecular orientation. However, it is important to note that this does not necessarily imply that the difference in molecular orientation alone gives rise to the apparent bright/dim contrast.

IV. CONCLUSION

Scanning tunneling microscopy and full-hemispherical x-ray photoelectron diffraction have been employed to study the interactions and film formation of C_{60} molecules deposited at the Cu(100) surface. The data reveal that in the evolution of C_{60} layers at room temperature the adsorbed molecules transport at the surface to decorate steps and form islands with local stripe patterns, which imply a reconstruction of the underlying substrate. A regular ordered monolayer film comprising a striped structure with two distinct C_{60} configurations is stabilized at higher temperatures (500–600 K). The two species exhibit different intramolecular contrast and corresponding orientations of C_{60} cages were determined. The system obeys the general trend of C_{60}/(metal surface) systems that quasihexagonal close-packed molecular islands and layers are formed with molecular next-neighbor distances close to that in the C_{60} van der Waals crystal.

[1] C. Cepek, I. Vobornik, A. Goldoni, E. Magnano, G. Selvaggi, J. Kröger, G. Panaccione, G. Rossi, and M. Sancrotti, Phys. Rev. Lett. **86**, 3100 (2001).

[2] R. Hesper, L. H. Tjeng, A. Heeres, and G. A. Sawatzky, Phys. Rev. Lett. **85**, 1970 (2000).

[3] M. R. C. Hunt, S. Modesti, P. Rudolf, and R. E. Palmer, Phys. Rev. B **51**, 10 039 (1995).

[4] T. Sakurai, X.-D. Wang, Q. K. Xue, Y. Hasegawa, T. Hashizume, and H. Shinohara, Prog. Surf. Sci. **51**, 263 (1996).

[5] A. V. Hamza, in *Fullerenes: Chemistry, Physics and Technology*,

edited by K. M. Kadish and R. S. Ruoff (Wiley, New York, 2000), p. 531.
[6] J. K. Gimzewski, S. Modesti, and R. R. Schlittler, Phys. Rev. Lett. **72**, 1036 (1994).
[7] R. Fasel, P. Aebi, R. G. Agostino, D. Naumov, J. Osterwalder, A. Santaniello, and L. Schlapbach, Phys. Rev. Lett. **76**, 4733 (1996).
[8] M. Ø. Pedersen, P. W. Murray, E. Laegsgaard, I. Stensgaard, and F. Besenbacher, Surf. Sci. **389**, 300 (1997).
[9] P. W. Murray, M. Ø. Pedersen, E. Laegsgaard, I. Stensgaard, and F. Besenbacher, Phys. Rev. B **55**, 9360 (1997).
[10] R. Fasel, R. G. Agostino, P. Aebi, and L. Schlapbach, Phys. Rev. B **60**, 4517 (1999).
[11] M. T. Cuberes, R. R. Schlittler, and J. K. Gimzewski, Appl. Phys. A: Mater. Sci. Process **66**, 669 (1998).
[12] C. Cepek, A. Goldoni, and S. Modesti, Phys. Rev. B **53**, 7466 (1996).
[13] M. Pedio, K. Hevesi, N. Zema, M. Capozi, P. Perfetti, R. Gouttebaron, J. J. Pireaux, R. Caudano, and P. Rudolf, Surf. Sci. **437**, 249 (1999).
[14] M. Pedio, R. Felici, X. Torrelles, P. Rudolf, M. Capozi, J. Rius, and S. Ferrer, Phys. Rev. Lett. **85**, 1040 (2000).
[15] J. Weckesser, J. V. Barth, and K. Kern, Phys. Rev. B **64**, 161403 (2001).
[16] J. Weckesser, C. Cepek, R. Fasel, J. V. Barth, F. Baumberger, T. Greber, and K. Kern, J. Chem. Phys. **115**, 9001 (2001).
[17] C. Rogero, J. I. Pascual, J. Gómez-Herrero, and A. M. Baró, J. Chem. Phys. **116**, 832 (2002).
[18] W. W. Pai, C.-L. Hsu, C. R. Chiang, Y. Chang, and K. C. Lin, Surf. Sci. **519**, L605 (2002).
[19] M. Grobis, X. Lu, and M. F. Crommie, Phys. Rev. B **66**, 161408 (2002).
[20] L.-F. Yuan, J. Yang, H. Wang, C. Zeng, Q. Li, B. Wang, J. G. Hou, Q. Zhu, and D. M. Chen, J. Am. Chem. Soc. **125**, 169 (2003).
[21] T. Hashizume, K. Motai, X. D. Wang, H. Shinohara, Y. Saito, Y. Maruyama, K. Ohno, Y. Kawazoe, Y. Nishina, H. W. Pickering, Y. Kuk, and T. Sakurai, Phys. Rev. Lett. **71**, 2959 (1993).
[22] A. V. Hamza and M. Balooch, Chem. Phys. Lett. **201**, 404 (1993).
[23] J. I. Pascual, J. Gómez-Herrero, C. Rogero, A. M. Baró, D. Sánchez-Portal, A. Artacho, P. Ordejón, and J. M. Soler, Chem. Phys. Lett. **321**, 78 (2000).
[24] H. Wang, C. Zeng, Q. Li, B. Wang, J. Yang, J. G. Hou, and Q. Zhu, Surf. Sci. **442**, L1024 (1999).
[25] A. W. Dunn, E. D. Svensson, and C. Dekker, Surf. Sci. **498**, 237 (2001).
[26] C. Cepek, R. Fasel, M. Sancrotti, T. Greber, and J. Osterwalder, Phys. Rev. B **63**, 125406 (2001).
[27] J. Osterwalder, P. Aebi, R. Fasel, D. Naumovic, P. Schwaller, T. Kreutz, L. Schlapbach, T. Abukawa, and S. Kono, Surf. Sci. **331–333**, 1002 (1995).
[28] E. I. Altman and R. J. Colton, Phys. Rev. B **48**, 18 244 (1993).
[29] E. Giudice, E. Magnano, S. Rusponi, C. Boragno, and U. Valbusa, Surf. Sci. **405**, L561 (1998).
[30] E. I. Altman and R. J. Colton, Surf. Sci. **279**, 49 (1992).
[31] T. David, J. K. Gimzewski, D. Purdie, L. B. Reihl, and R. R. Schlittler, Phys. Rev. B **50**, 5810 (1994).
[32] J. E. Rowe, P. Rudolf, L. H. Tjeng, R. A. Malic, F. Meigs, C. T. Chen, and E. W. Plummer, Int. J. Mod. Phys. B **6**, 3909 (1992).
[33] A. J. Maxwell, P. A. Brühwiler, S. Andersson, D. Arvanitis, B. Hernnäs, O. Karis, D. C. Mancini, N. Martensson, S. M. Gray, M. K.-J. Johansson, and L. S. O. Johansson, Phys. Rev. B **52**, 5546 (1995).
[34] M. K.-J. Johansson, A. J. Maxwell, S. M. Gray, P. A. Brühwiler, D. C. Mancini, L. S. O. Johansson, and N. Mårtensson, Phys. Rev. B **54**, 13 472 (1996).
[35] R. Fasel, P. Aebi, J. Osterwalder, L. Schlapbach, R. G. Agostino, and G. Chiarello, Phys. Rev. B **50**, 14 516 (1994).